

# A Frequency-Domain Analysis of Haptic Gratings

Steven A. Cholewiak, Kwangtaek Kim, Hong Z. Tan, *Senior Member, IEEE*, and Bernard D. Adelstein, *Member, IEEE*

**Abstract**—The detectability and discriminability of virtual haptic gratings were analyzed in the frequency domain. Detection (Exp. 1) and discrimination (Exp. 2) thresholds for virtual haptic gratings were estimated using a force-feedback device that simulated sinusoidal and square-wave gratings with spatial periods from 0.2 to 38.4 mm. The detection threshold results indicated that for spatial periods up to 6.4 mm (i.e., spatial frequencies  $>0.156$  cycle/mm), the detectability of square-wave gratings could be predicted quantitatively from the detection thresholds of their corresponding fundamental components. The discrimination experiment confirmed that at higher spatial frequencies, the square-wave gratings were initially indistinguishable from the corresponding fundamental components until the third harmonics were detectable. At lower spatial frequencies, the third harmonic components of square-wave gratings had lower detection thresholds than the corresponding fundamental components. Therefore, the square-wave gratings were detectable as soon as the third harmonic components were detectable. Results from a third experiment where gratings consisting of two superimposed sinusoidal components were compared (Exp. 3) showed that people were insensitive to the relative phase between the two components. Our results have important implications for engineering applications, where complex haptic signals are transmitted at high update rates over networks with limited bandwidths.

**Index Terms**—Detection, discrimination, frequency-domain analysis, haptic gratings, complex-waveform discrimination.

## 1 INTRODUCTION

MANY studies of human texture perception, including our own, have employed sinusoidal texture models for the reason that any surface height function representing texture can be decomposed into a series of sinusoidal functions using Fourier analysis [1], [2], [3]. The implicit hypotheses in these studies have been that

1. The human somatosensory system may be capable of performing a spectrum analysis of the proximal stimuli arising from interacting with a textured surface.
2. The perception of individual spectral components may be superimposed to form an overall percept.

That these hypotheses may have some validity for perception has been suggested by studies in vision [4] and touch [5], [6], [7]. Using gratings of sinusoidal, square, rectangular, and sawtooth waveforms displayed on a CRT monitor, Campbell and Robson [4] obtained evidence for a linear system model of visual perception that operates within a limited range of frequencies. Among the studies of the

somatosensory system, a four-channel model for touch perception was proposed to account for the full range of vibratory sensitivity based on neurophysiological and psychophysical evidence [8], [9]. More recently, it was suggested that the Pacinian system consists of a set of “frequency-tuned minichannels” that conveys information about the spectral components in a complex waveform, despite the fact that all Pacinian afferents have a homogeneous spectral profile in terms of their response to stimuli over a wide range of frequencies [7]. While these researchers have been interested in the perception of vibrations and how surface textures are conveyed through vibrations [10], we have also been interested in the rendering of virtual textured surfaces [3], [11], [12], [13], [14]. Instead of constructing polyharmonic waveforms by adding sinusoidal components of various frequencies, we have used triangular, square-wave, and sinusoidal gratings (tactile analog of the visual gratings used in the Campbell and Robson study [4]) to represent virtual surface textures. The unique complexities of square and triangular waveforms in terms of the fundamental and harmonic components and their relative amplitudes allow us to make specific and quantitative predictions about how they will be perceived based on a linear model of the somatosensory system. (See [15], pp. 1263-1264, for an excellent discussion on the use of Fourier analysis to study the perception of complex patterns in touch).

In the present study, we used virtual haptic surfaces with sinusoidal and square-wave gratings to analyze the detectability and discriminability of the gratings in the frequency domain. Three experiments were conducted. Exps. 1 and 2 measured the detection and discrimination thresholds for the sinusoidal and square-wave gratings at a series of spatial periods/frequencies. In the detection experiment (Exp. 1), we compared the measured detection thresholds for square-wave gratings to the thresholds predicted from

- S.A. Cholewiak is with the Department of Psychology, Rutgers University, New Brunswick, Piscataway, NJ 08854-8020. E-mail: scholewi@eden.rutgers.edu.
- K. Kim and H.Z. Tan are with the Haptic Interface Research Laboratory, Purdue University, 465 Northwestern Avenue, West Lafayette, IN 47907-2035. E-mail: {samuelkim, hongtan}@purdue.edu.
- B.D. Adelstein is with the Human Systems Integration Division, NASA Ames Research Center, Moffett Field, CA 94035-1000. E-mail: Bernard.D.Adelstein@nasa.gov.

Manuscript received 25 July 2008; revised 25 Feb. 2009; accepted 22 June 2009; published online 11 Aug. 2009.

Recommended for acceptance by A. Okamura.

For information on obtaining reprints of this article, please send e-mail to: toh@computer.org, and reference IEEECS Log Number TH-2008-07-0049. Digital Object Identifier no. 10.1109/ToH.2009.36.

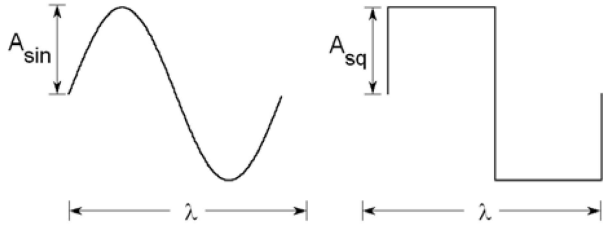


Fig. 1. The sinusoidal and square-wave gratings used in the present study. Shown are one cycle of each waveform, respectively, where  $A$  denotes the half peak-to-peak amplitude and  $\lambda$  the spatial period of the waveforms. (Modified from [29, Fig. 1 ], © 2007 IEEE)

the detectability of the corresponding fundamental and harmonic sinusoidal components using the thresholds measured for sinusoidal gratings. In the discrimination experiment (Exp. 2), we measured the discrimination thresholds for pairs of sinusoidal and square-wave gratings with covarying amplitudes such that the amplitude of the sinusoidal grating always matched that of the fundamental component of the square-wave grating. Finally, we measured the discriminability of gratings consisting of two superimposed sinusoidal components with different relative phases (Exp. 3).

We outline the main idea of the present study as follows: Let us consider two gratings, one sinusoidal and one square-wave, with the same amplitude (see Fig. 1). The height map of the sinusoidal grating is defined by

$$h_{\sin}(x) = A_{\sin} \sin(2\pi x/\lambda) \quad (1)$$

and that of the square-wave gratings is

$$h_{sq}(x) = \begin{cases} A_{sq} & \text{if } \sin(2\pi x/\lambda) > 0, \\ -A_{sq} & \text{if } \sin(2\pi x/\lambda) < 0, \end{cases} \quad (2)$$

where  $A_{\sin}$  and  $A_{sq}$  denote the half peak-to-peak amplitude of the sinusoidal and square waveforms, respectively,  $x$  denotes the  $x$ -position along which surface height ( $h$ ) varies, and  $\lambda$  denotes the spatial period of the virtual gratings. These gratings are perceived as surface textures with the parameter values chosen in the present study.

The Fourier expansion of the square-wave grating shown in (2) is

$$h_{sq}(x) = A_{sq} \left( \frac{4}{\pi} \right) \sum_{n=1,3,5,\dots}^{\infty} \frac{1}{n} \sin\left(n \frac{2\pi x}{\lambda}\right), \quad (3)$$

which can be expanded as

$$h_{sq}(x) = A_{sq} \left( \frac{4}{\pi} \right) \left\{ \begin{array}{l} \sin\left(\frac{2\pi x}{\lambda}\right) \\ + \frac{1}{3} \sin\left(3 \frac{2\pi x}{\lambda}\right) \\ + \frac{1}{5} \sin\left(5 \frac{2\pi x}{\lambda}\right) \\ + \dots \end{array} \right\}. \quad (4)$$

Therefore, given a sinusoidal grating and a square-wave grating with the same overall amplitude ( $A_{\sin} = A_{sq}$ ), the amplitude of the fundamental component of the square-wave grating is larger than that of the sinusoidal grating by a factor of  $4/\pi$ . The harmonic components of the square-wave have smaller amplitudes than that of the

fundamental component, as indicated by the coefficients  $4/(3\pi)$ ,  $4/(5\pi)$ , etc.

If we hypothesize that the spectral components described in (4) can be perceived individually and be superimposed as would a linear system, then the detectability of a square-wave grating should be determined by the amplitude of its most detectable component, or equivalently, the component with the lowest detection threshold. The detectability of the components can be determined by the detection thresholds for sinusoidal gratings at the corresponding spatial period/frequency, after taking into account the coefficients in (4) (e.g.,  $4/\pi$  for the fundamental component,  $4/(3\pi)$  for the third harmonic, etc.). It should now be clear that once the detection thresholds for sinusoidal gratings have been measured, the relative detectability of the spectral components in a square-wave grating can be calculated according to (4). The predicted relative detectability can then be compared with the experimentally measured detection thresholds for square-wave gratings. For example, suppose we have determined that the fundamental component of a square-wave at spatial period  $\lambda$  has the lowest detection threshold among all the spectral components. We can then predict that the detection threshold for a square-wave grating at spatial period  $\lambda$  should be  $\pi/4$  times the amplitude threshold of the sinusoidal grating at the same spatial period. Likewise, if the third harmonic component has a lower detection threshold than that of the fundamental component, then the detection threshold for a square-wave grating should be  $3\pi/4$  times that of the sinusoidal grating, as dictated by the coefficients in (4).

In the present study, we hypothesized that, as the amplitude of a square-wave grating increased, its fundamental component was detected first, followed by the detection of its third harmonic component, etc. We then predicted that

*Hypothesis 1:* The detectability of the square-wave grating could be quantitatively predicted from the detectability of its fundamental component.

*Hypothesis 2:* The square-wave grating could not be distinguished from its fundamental component until its harmonic components were detectable.

Furthermore, if the somatosensory system processes complex signals in the spectral domain instead of the temporal or spatial domain, then the square-wave grating, shown in Fig. 1, should not feel any different from a grating that has the same spectral components as listed in (4) but with different phase characteristics for the harmonics. This led to one more prediction that

*Hypothesis 3:* The perception of a grating consisting of two superimposed sinusoidal components does not depend on the relative phase of the two components.

Three experiments were conducted to test the three hypotheses, respectively. In Section 2, we describe the experimental apparatus and discuss its performance. In Sections 3, 4, and 5, we present the methods and findings of Exps. 1-3, respectively. A general discussion in Section 6 concludes the paper.

## 2 THE MINISTICK

A custom-designed, high position-resolution, 3-DOF (degrees of freedom) force-feedback device, the "ministick"

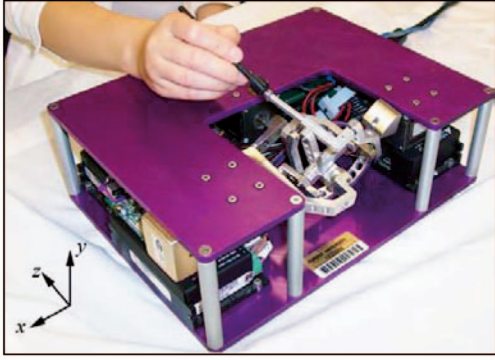


Fig. 2. The ministick, a 3-DOF force-feedback device used to render virtual gratings in the present study. (From [29, Fig. 2], © 2007 IEEE)

(see Fig. 2), was used in all the experiments. A user interacts with virtual objects rendered by the ministick using a stylus (see Fig. 2) that is magnetically connected to the end effector of the ministick. Results from earlier studies have shown that the discrimination thresholds using real texture samples and virtual textures simulated on the ministick were very similar, thereby indicating that the ministick appears to be an appropriate device for studying haptic texture perception [13], [14].

The ministick is a passively balanced haptic device based on a multiloop parallel mechanism invented by Adelstein [16] and custom-built by the University of California Berkeley, with an embedded controller designed and implemented by Traylor [17]. Detailed documentation of the ministick, shown in Fig. 2, can be found in Traylor’s Master’s thesis [17]. The ministick has a usable, interference-free, bowl-shaped hemispherical workspace measuring approximately 9 cm × 9 cm × 6 cm. A key advantage of the ministick for the present study is its position resolution, which is achieved through the use of 409,600-count-per-revolution, sinusoidally interpolated optical encoders (cf., [17, Section 4.5]). It is capable of an update rate of 3.8 kHz and has a position resolution of ~1.5 μm and velocity resolution of ~3 mm/sec at the center of its workspace. Under the simplest form of impedance control (i.e., proportional displacement feedback), the ministick produces a stable 8 N/mm stiffness at its typical update rate of 2 kHz. The theoretical nominal endpoint force resolution is 0.0021 N, which changes with linkage pose and endpoint location.

The ministick’s position resolution was validated by a calibrated stepper motor stage (model UT100 linear stage, Klinger Micro-Controle S.A./Newport Corporation), geared for 0.1 μm step size. The stage provided controlled, known displacements against which the ministick encoder values could be compared. The setup of the apparatus is shown in Fig. 3.

The validation was carried out (roughly) along the x-axis of the ministick coordinate system, the direction in which participants stroked the virtual gratings in the present study. The stepper motor stage was rigidly attached to the top end of the stylus used in the study (see Fig. 2). The bottom end of the stylus was connected, in turn, to the ministick linkage via its standard spherical magnetic coupling (see Fig. 3). The stepper motor was commanded to make ten 0.1-μm steps at a

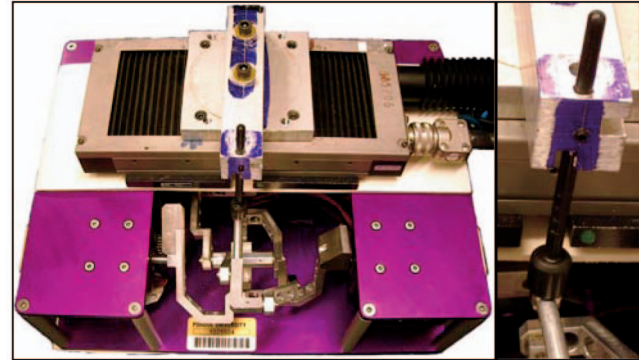


Fig. 3. (a) Hardware setup for the validation of the ministick position resolution. (b) A close-up view of the mechanical connection between the stepper motor stage and the ministick linkages.

time. The resultant  $x, y, z$  displacements of the ministick’s haptic interaction point (i.e., the center of the spherical coupling at the bottom end of the stylus) were computed from the ministick encoders and recorded at an update rate of 2 kHz.

The validation results are shown in Fig. 4. The “+” symbols show the euclidean distance relative to the starting point (the initial  $x, y, z$  reading), computed from the ministick encoders, as a function of the stepper motor displacement. The solid line shows a straight line with a unity slope representing ideal, perfect measurement. The data were fit to a straight line with a slope of 0.99 and an intercept of  $-1.3 \mu\text{m}$  ( $R^2 = 0.9986$ ). Therefore, over the 60 μm displacement range tested, the accuracy of the ministick is 1.3 μm. With its theoretical 1.5 μm position resolution, the actual resolution of the ministick in the tested range is estimated to be  $1.5/0.99 \approx 1.5 \mu\text{m}$ .

### 3 EXPERIMENT 1: DETECTION OF SINUSOIDAL AND SQUARE-WAVE GRATINGS

The purpose of this experiment was to measure the amplitude detection thresholds for sinusoidal and square-wave gratings in order to test the hypothesis that the detectability of a square-wave grating can be predicted from the detectability of its fundamental components.

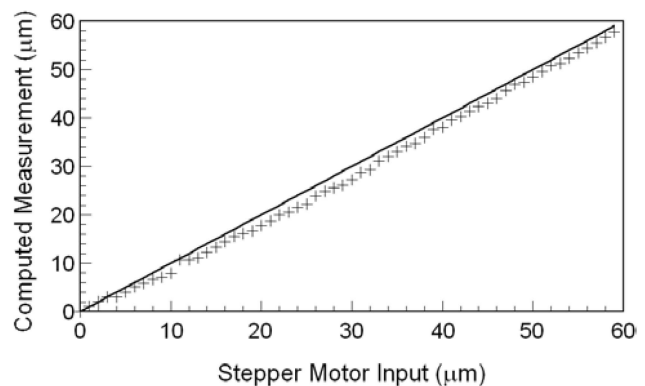


Fig. 4. Ministick position-resolution calibration results. The measured versus controlled displacements (“+” symbols) are shown, with the solid straight line indicating perfect measurement.

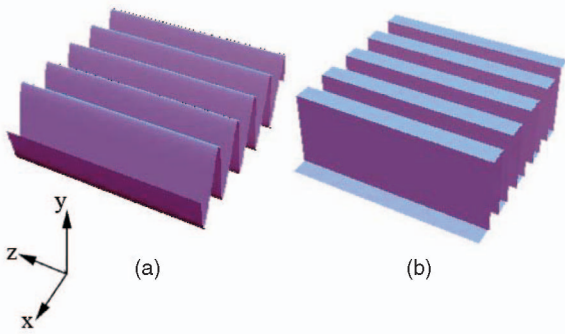


Fig. 5. Three-dimensional illustrations of the (a) sinusoidal and (b) square-wave gratings used in the present study. The amplitudes are exaggerated for illustrative purpose.

### 3.1 Participants

Five participants (3 males and 2 females, age range 22-41 years old, average age 28.2 years old) took part in the experiment. Four (P1, P2, P4, and P5) were right-handed and one (P3) was left-handed by self-report.

Participants P1, P2, and P4 had previous experience with haptic interfaces and perception experiments. Participants P3 and P5 received compensation for their experimental time. The participants gave their written consent to the experimental protocol that had been approved by the Institutional Review Board at Purdue University.

### 3.2 Stimuli

Virtual textures with sinusoidal and square-wave gratings were generated on the ministick. The surface height profiles of these gratings varied along the  $x$ -axis of the ministick coordinate frame but remained constant along the  $z$ -axis. Fig. 5 shows an example of the sinusoidal and square-wave textured surfaces used in the present study in a coordinate frame that is consistent with that shown in Fig. 2. The actual amplitudes of the haptic virtual gratings were on the order of microns or tens of microns. The drawings in Fig. 5 are, therefore, scaled versions for illustrative purpose only.

The height map  $h(x)$  of the sinusoidal and square-wave gratings was defined by (1) and (2) shown earlier. The restoring force was then calculated for both grating types as follows:

$$F_y = \begin{cases} K \times [h(x) - y], & \text{if } y < h(x), \\ 0, & \text{if } y \geq h(x), \end{cases} \quad (5)$$

where  $y$  denotes the vertical position (along the  $y$ -axis) of the ministick stylus tip (modeled as an infinitesimally small point) and  $K$  denotes the stiffness coefficient ( $K = 2.0 \text{ N/mm}$  in all conditions). It follows that the restoring force was always pointing up, i.e., along the positive direction of the  $y$ -axis of the ministick coordinate frame. No forces along the  $x$  or  $z$  direction were rendered (hence, no frictional forces were simulated either).

Eight spatial periods for both grating types were used in Exp. 1: 25.6, 12.8, 6.4, 3.2, 1.6, 0.8, 0.4, and 0.2 mm. They corresponded to the spatial frequencies of 0.039, 0.078, 0.156, 0.313, 0.625, 1.25, 2.5, and 5 c/mm (cycles per millimeter), respectively. This range was selected to include spatial periods that would provide a wide variety of spatial and temporal frequencies within the constraints of the resolution and workspace of the ministick.

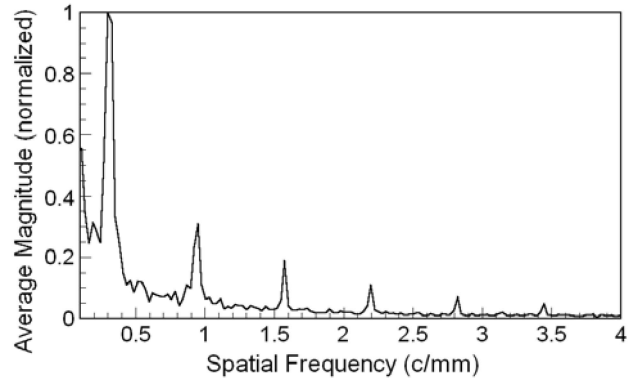


Fig. 6. Normalized FFT magnitude of position data recorded during stroking of a square-wave grating ( $\lambda = 3.2 \text{ mm}$ ,  $A_{sq} = 35 \mu\text{m}$ ). Note that the relative amplitudes of the spectral components at the fundamental frequency and the harmonics follow the coefficients in (4) closely.

### 3.3 Verification of Square-Wave Gratings

It is generally undesirable to render “sharp” force changes by a force-feedback device as was required in the present study by the rendering of square-wave gratings. However, we observed no “buzzing” noise or device instability when the gratings were presented at levels close to detection thresholds ( $<10 \mu\text{m}$  for square-wave gratings). Furthermore, a spectral analysis of the recorded  $y$  versus  $x$  position data verified that the relative amplitudes of the spectral components of a square-wave grating followed the coefficients in (4) closely. Fig. 6 shows the normalized magnitude of the Fourier transform of the  $y(x)$  position data recorded while a user stroked a square-wave grating with a spatial period of  $\lambda = 3.2 \text{ mm}$  and a suprathreshold amplitude of  $A_{sq} = 35 \mu\text{m}$ . It can be seen that the fundamental component is at a spatial frequency of 0.313 c/mm, as expected. The harmonic components appear near 0.938 (3rd), 1.563 (5th), 2.188 (7th), 2.813 c/mm (9th), etc. The amplitudes of the harmonic components are about 1/3, 1/5, 1/7, 1/9, etc., of that of the fundamental component (normalized to 1). Fig. 6 therefore provides evidence that the virtual gratings rendered by the ministick could be perceived by the participants through variations in the stylus’s  $y$ -position.

Similar analyses of the temporal data  $y(t)$  indicated a lack of distinct spectral peaks in the Fourier transform, presumably due to the “smearing” caused by variable stroking velocities. Fig. 7 compares the average FFT magnitudes of the same sequence of recorded  $y$ -position data analyzed in the spatial domain (top panel) and temporal domain (bottom panel), respectively. While the spatial spectrum shows distinctive peaks at expected locations, the temporal spectrum does not. Recorded force-command data exhibited similar patterns although the spatial spectral peaks were not as pronounced, which was consistent with the results from our earlier studies (e.g., [3], [11], [12]). In the rest of this paper, we report all results in the spatial, not temporal, domain (see also our earlier work demonstrating that the detection of torque variations depends on the spatial, not temporal, specification of the torque profiles [18]).

### 3.4 Procedure

A three-interval, forced-choice, one-up three-down adaptive procedure was employed [19], [20]. On each trial, the

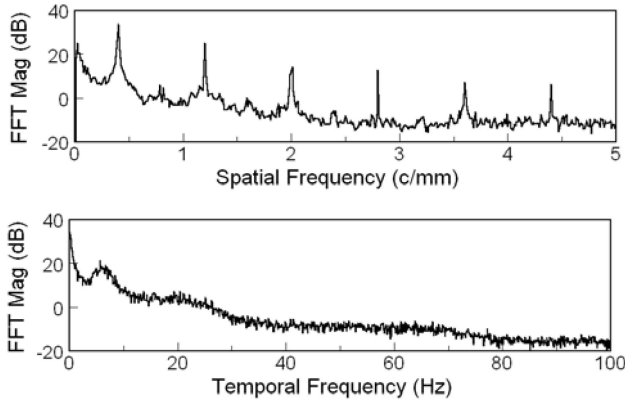


Fig. 7. Spatial (top) and temporal (bottom) FFT magnitudes for  $y$ -position of the ministick stylus, recorded when a participant stroked a square-wave grating with  $\lambda = 2.5$  mm and  $A_{sq} = 50$   $\mu\text{m}$ .

participants received three presentations of stimuli (three intervals). During two of the three intervals on each trial, a nontextured flat surface (i.e.,  $A = 0$ ) was presented. A textured surface was presented in the remaining interval, which was randomly selected to be the first, second, or third interval with equal a priori probabilities. The participants were instructed to report the interval ("1," "2," or "3") in which they felt a texture. Thus, we tested the participants' ability to detect the presence of a texture grating on a flat surface.

The amplitude of the textured surfaces was adjusted according to the correctness of the participant's responses. On the first trial of each session, the initial amplitude was chosen to be approximately 20 dB above the expected threshold level to ensure that the participants could clearly perceive the stimulus. The amplitude level was decreased after three consecutive correct responses and was increased after one incorrect response. Initially, the amplitude level increased or decreased by a factor of 4. The relatively large step size allowed the participants to approach their thresholds quickly, facilitating convergence. A reversal occurred when the amplitude level changed from increasing to decreasing or vice versa. After the first three reversals, the amplitude level changed by a factor of 1.25. The smaller step size improved the precision of the threshold estimates. The experimental session was terminated after 12 reversals at the smaller step size. The number of trials in each session varied, but was typically within 60-80 trials (see Fig. 8 for a typical session). Each session lasted 10-15 min. The participant was asked to repeat a session if the data failed to converge as judged by the experimenter.

The participants were comfortably seated before a computer screen and a keyboard with the dominant arm rested on a comfortable support. There was very little perceptible sound when stroking the textures gratings. Nevertheless, the participants wore sound attenuating earmuffs to eliminate any possible auditory cues. The participant grasped the probe of the ministick by the dominant hand in the same way that s/he would normally hold a pencil. Initial training was provided where a series of representative stimuli was presented to familiarize the participant with the virtual textured surfaces. The participants were instructed to explore within the center of the

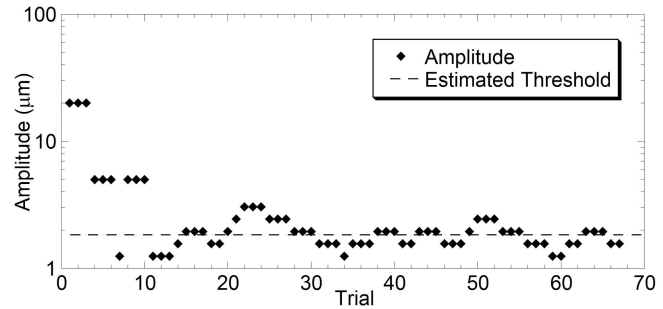


Fig. 8. A typical session of the adaptive tracking procedure. The stimulus amplitude (filled diamonds) as a function of trial number and the estimated threshold (dashed line) are shown.

ministick's workspace to avoid the nonlinear device behavior at the boundaries of the workspace. For each waveform and spatial period, the participants were encouraged to experiment with and then use the optimal stroking speed that seemed to facilitate the detection or discrimination of the virtual gratings.

The first interval in a trial was initiated by a keystroke on the computer keyboard. The participants were then allowed to move the stylus freely, from side to side, to stroke the virtual surface. When the participant was ready to move on, additional keystrokes initiated the second, then the third intervals. The response was recorded by a final keystroke on the number 1, 2, or 3 keys, which initiated the next trial. As is typical with threshold studies, no feedback was provided. The participants were allowed to take a brief break between experimental sessions.

Two types of grating waveforms, sinusoidal and square-wave, were used. Participants P1-P3 were tested with sinusoidal gratings first. Because the thresholds for square-wave gratings were found to be lower than those for sinusoidal gratings, additional data on sinusoidal gratings were collected for participants P1-P3 after the initial testing to examine possible learning effects. The order of the spatial frequencies was randomized per waveform for participants P1-P3. Participants P4 and P5 were tested with a randomized order of waveform and frequency. A total of 16 threshold estimates (2 waveforms  $\times$  8 frequencies per waveform) were collected per participant. In the cases where more than one estimate were obtained for the purpose mentioned above or because a participant's performance failed to converge, the lowest threshold for the waveform  $\times$  frequency combination was used in data analysis.

### 3.5 Data Analysis

For each spatial frequency, thresholds were calculated from the peak and valley amplitude values over the last 12 reversals at the smaller step size. Specifically, six threshold values were estimated by averaging the six pairs of peak/valley amplitude values recorded during the last 12 reversals. The mean and the standard error for the detection threshold were then calculated from the six threshold estimates. According to Levitt [19], the resulting thresholds converged on the psychometric function at the 79.4 percentile level.

For each pair of detection thresholds for sinusoidal and square-wave gratings at the same spatial frequency, a ratio

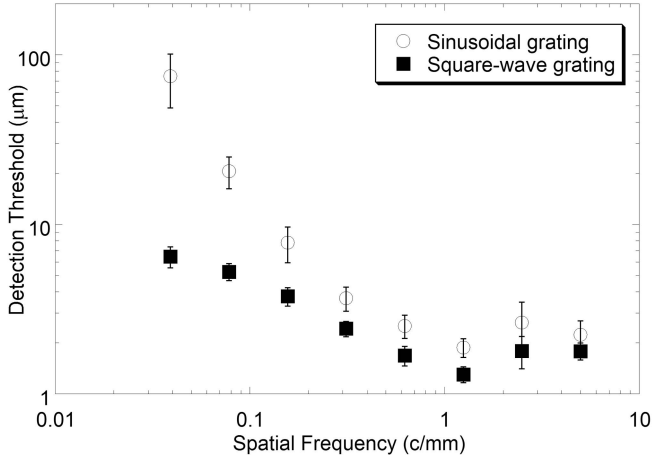


Fig. 9. Detection thresholds for sinusoidal and square-wave gratings in Exp. 1. The averages and standard errors are shown. (Modified from [29, Fig. 3], © 2007 IEEE)

of the former over the latter was calculated. The ratios were then compared to  $4/\pi$ , the coefficient shown in (4), to investigate the extent to which the threshold for the sinusoidal grating matched that for the fundamental component of the corresponding square-wave grating.

### 3.6 Results

The average detection thresholds are shown in Fig. 9 as a function of spatial frequency. It is apparent that the thresholds for the square-wave gratings (filled squares) were always lower than those for the sinusoidal gratings (open circles) at all the spatial frequencies tested. For both types of waveforms, thresholds decreased as spatial frequency increased and then increased again. The threshold values ranged from  $1.1 \mu\text{m}$  (S3, at  $5 \text{ c/mm}$ ) to  $183.1 \mu\text{m}$  (S2, at  $0.039 \text{ c/mm}$ ) (average  $14.5 \pm 31.3 \mu\text{m}$ ) for the sinusoidal gratings, and from  $0.9 \mu\text{m}$  (S5, at  $5 \text{ c/mm}$ ) to  $8.7 \mu\text{m}$  (S2, at  $0.039 \text{ c/mm}$ ) (average  $3.1 \pm 2.1 \mu\text{m}$ ) for the square-wave gratings. It can be observed that the difference between the thresholds for the sinusoidal and square-wave gratings at the same spatial frequency decreased asymptotically as spatial frequency increased. A two-way ANOVA with the factors Waveform (sinusoidal and square-wave) and Frequency (8 values) confirmed that both factors were significant (Waveform:  $F(1,464) = 71.064, p < 0.001$ ; Frequency:  $F(7,464) = 48.658, p < 0.001$ ). The ANOVA also indicated a highly significant interaction between Waveform and Frequency ( $F(7,464) = 37.463, p < 0.001$ ).

Fig. 10 shows the ratios of the thresholds for sinusoidal gratings over those for square-wave gratings at the corresponding spatial frequencies. The dashed line corresponds to  $4/\pi$  or 1.273, i.e., the predicted ratio if the detectability of a square-wave grating was determined by that of its fundamental component. It appears that the ratios did not deviate significantly from the predicted value except at the lowest spatial frequencies tested. A one-way ANOVA with Frequency as the fixed factor confirmed that Frequency was a significant factor ( $F(7,32) = 9.730, p < 0.001$ ). One-sample t-tests were performed to compare the ratios to  $4/\pi$ . The results showed that the ratios at the six highest spatial frequencies ( $0.156 - 5 \text{ c/mm}$ ) were not significantly different

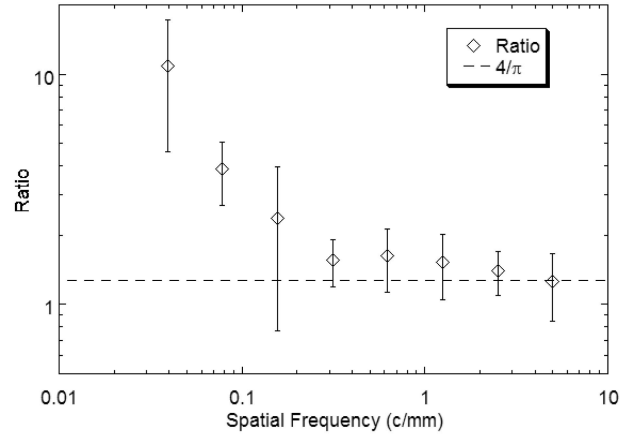


Fig. 10. Ratios (open diamonds) of the detection thresholds for sinusoidal gratings over the thresholds for square-wave gratings at the corresponding spatial frequencies. The averages and standard deviations are shown. (Modified from [29, Fig. 4], © 2007 IEEE)

from  $4/\pi$  ( $(t, p) = (1.532, 0.200), (1.760, 0.153), (1.603, 0.184), (1.178, 0.304), (0.944, 0.399),$  and  $(-0.091, 0.932)$ , respectively), and that only the ratios at the two lowest spatial frequencies ( $0.039$  and  $0.078 \text{ c/mm}$ ) were significantly different from  $4/\pi$  ( $(t, p) = (3.433, 0.026), (4.880, 0.008)$ , respectively). In addition, one-sample t-tests were performed to compare the ratios to 1. The results showed that the ratios at five spatial frequencies ( $0.039, 0.078, 0.313, 0.625,$  and  $2.5 \text{ c/mm}$ ) were significantly different from 1 ( $(t, p) = (3.530, 0.024), (5.391, 0.006), (3.463, 0.026), (2.824, 0.048),$  and  $(2.971, 0.041)$ , respectively), and those at the remaining three frequencies ( $0.156, 1.25,$  and  $5 \text{ c/mm}$ ) were not significantly different from 1 ( $(t, p) = (1.913, 0.128), (2.439, 0.071),$  and  $(1.397, 0.235)$ , respectively).

### 3.7 Discussion

In this experiment, we estimated the detection thresholds for sinusoidal and square-wave gratings superimposed on a flat surface. The thresholds were compared by taking the ratio of the threshold for a sinusoidal grating over the threshold for a square-wave grating at the same spatial frequency. Since the fundamental component of a square waveform has an amplitude that is  $4/\pi$  times that of the square-wave (see (4)), we reasoned that the detection threshold for a purely sinusoidal waveform would be  $4/\pi$  times that for a square-wave *if* the square-wave was detected by sensing its fundamental component alone. Results from the five participants showed that the detection thresholds for sinusoidal gratings were indeed greater than those for square-wave gratings. Furthermore, the threshold ratios were indeed around  $4/\pi$  at the higher spatial frequencies tested.

We then asked why the threshold ratios were higher than  $4/\pi$  at the lower spatial frequencies tested. Our hypothesis was that at the lower frequencies, the higher harmonics of the square-wave gratings were detectable at an amplitude (of the square-wave) where the fundamental component could not be detected yet. Therefore, the amplitude of the square-wave upon its detection was below that predicted by the detection of its fundamental component, hence the  $>4/\pi$  ratio. This led to the prediction that at higher spatial frequencies, when the waveform amplitudes are small, a square-wave grating should be

indistinguishable from a sinusoidal grating at its fundamental frequency because the square-wave's harmonics are undetectable yet. In fact, the amplitude at which a square-wave grating feels different from a sinusoidal grating should be predictable from the detection threshold of the square-wave's third harmonic component. This led to the second experiment, where the participants were asked to distinguish a square-wave grating from a sinusoidal grating at the same fundamental frequency.

## 4 EXPERIMENT 2: DISCRIMINATION OF SINUSOIDAL AND SQUARE-WAVE GRATINGS

The purpose of the second experiment was to measure the discrimination thresholds for sinusoidal and square-wave gratings covarying in amplitude. We wanted to test the hypothesis that as the amplitude increased, discrimination of the two waveforms was not possible until the harmonic components of the square-wave gratings were above human detection thresholds.

### 4.1 Methods

The methods for Exp. 2 were very similar to those used in Exp. 1: the same five participants took part in Exp. 2 and the same three-interval, forced-choice, one-up three-down adaptive procedure was used. The main differences between Exps. 1 and 2 are outlined below.

As in Exp. 1, the participants received three presentations of stimuli on each trial. Unlike in Exp. 1, however, a sinusoidal grating was presented during two of the intervals, and a square-wave grating was presented in the remaining intervals. The interval containing the square-wave grating was chosen randomly to be the first, second, or third interval. Participants were told to report the interval ("1," "2," or "3") that felt different from the other two (i.e., the interval containing the square-wave grating).

Seven spatial periods for both grating types were used: 38.4, 19.2, 9.6, 4.8, 2.4, 1.2, and 0.6 mm. They corresponded to the spatial frequencies of 0.026, 0.052, 0.104, 0.208, 0.417, 0.833, and 1.667 c/mm, respectively. The seven spatial periods were chosen to be three times those tested in Exp. 1, except that the longest spatial period of 76.8 mm ( $3 \times 25.6$  mm) was not used because it required stroking displacements that were much larger than those typically utilized by the participants and multiple cycles of the grating would have exceeded the ministick's usable workspace. Consequently, the spatial frequencies tested in Exp. 2 were a third of those tested in Exp. 1. This made it possible for us to use the thresholds obtained from Exp. 1 to predict the detectability of the third harmonic of the square-wave gratings tested in Exp. 2.

For each pair of sinusoidal and square-wave gratings presented during the three intervals of a trial, the amplitude of the square-wave surface was reduced by a factor of  $\pi/4$  to equalize the amplitude of the fundamental component of the square-wave grating to that of the sinusoidal grating. With this adjustment in amplitude, a square-wave grating would feel the same as a sinusoidal grating of the same spatial frequency as long as the amplitudes of the square-wave harmonic components were smaller than their respective detection thresholds. When the waveform

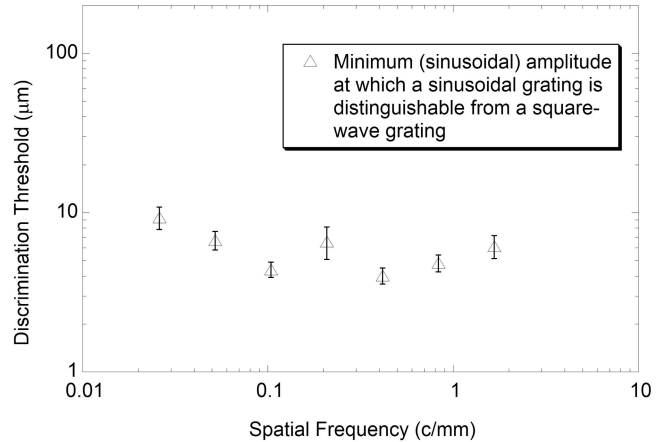


Fig. 11. Amplitude discrimination thresholds from Exp. 2 for the sinusoidal gratings. The minimum sinusoidal grating amplitudes at which participants could feel the difference between a pair of sinusoidal and square-wave gratings at the same spatial frequency are shown. Also, the standard errors are shown. The corresponding square-wave grating amplitudes would be the thresholds shown here multiplied by  $\pi/4$ .

amplitudes were increased or decreased according to the one-up three-down adaptive rules, the ratio between the amplitudes of the square-wave and the sinusoidal gratings was always kept constant at  $\pi/4$  to ensure that the amplitude of the sinusoidal grating was always the same as that of the fundamental component of the square-wave grating on any particular trial. Each participant completed a total of 7 sessions, providing one discrimination threshold for each spatial frequency. Each estimated threshold was the amplitude of the *sinusoidal* grating at which the participant could feel the difference between the pair of sinusoidal and square-wave gratings. We then calculated the corresponding amplitude of the third harmonic component of the square-wave and compared it to the detection thresholds obtained from Exp. 1 at the same spatial frequency as the third harmonic. To the extent that the third harmonic was indeed at its detection threshold level when the pair of sinusoidal and square-wave gratings became discriminable, we could then conclude that a square-wave grating felt different from a sinusoidal grating only when its third and higher harmonic components were above human detection thresholds.

The total experimental time for each participant to complete all spatial frequencies for both Exps. 1 and 2 ranged from 6 to 9 hours.

### 4.2 Results

Fig. 11 shows the average discrimination thresholds as a function of spatial frequency. The thresholds generally followed a U-shaped trend. The thresholds averaged  $6.0 \pm 2.8$   $\mu\text{m}$  for the five participants, with the lowest threshold being 1.8  $\mu\text{m}$  (S5, at 0.417 c/mm) and the highest threshold 15.6  $\mu\text{m}$  (S4, at 0.208 c/mm). A one-way ANOVA with Frequency (7 values) as the fixed factor confirmed that Frequency was a significant factor ( $F(6,203) = 19.240$ ,  $p < 0.001$ ). The elevated average at 0.208 c/mm was due to the relatively higher thresholds of P3 and P4 (9.4 and 10.7  $\mu\text{m}$ , respectively). The average threshold for P1, P2,

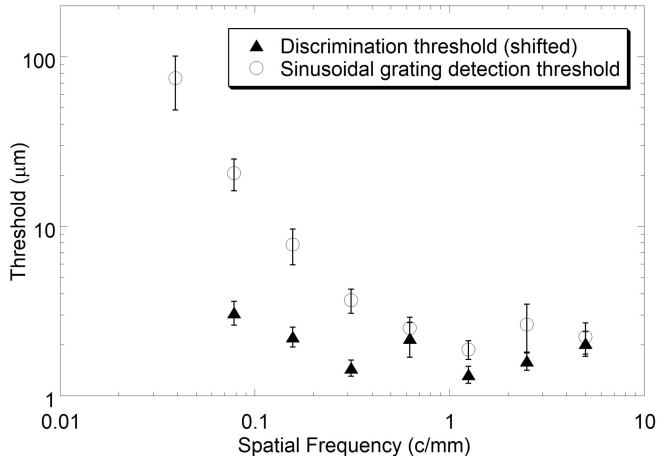


Fig. 12. Comparison of the detection thresholds obtained from Exp. 1 (open circles, replotted from Fig. 9) and the discrimination thresholds obtained from Exp. 2 (filled triangles). The latter was shifted by 3 in frequency and by 1/3 in amplitude. The standard errors are shown.

and P5 was  $4.3 \mu\text{m}$ , which was more consistent with the general trend of the data.

The discrimination thresholds were then compared to the detection thresholds obtained from Exp. 1. To clarify how the discrimination and detection thresholds were compared, let us consider the average discrimination threshold at the spatial frequency of  $1.667 \text{ c/mm}$  (spatial period  $0.6 \text{ mm}$ ), which was  $6.1 \mu\text{m}$  for the sinusoidal grating (see Fig. 11). The corresponding amplitude threshold for the square-wave grating at  $1.667 \text{ c/mm}$  would be  $6.1 \times \pi/4 = 4.8 \mu\text{m}$ , taking into account the coefficient in (4). It follows that, when the participants were barely able to discriminate the sinusoidal and square-wave gratings at  $1.667 \text{ c/mm}$ , the amplitude of the third harmonic component (at  $1.667 \text{ c/mm} \times 3 = 5 \text{ c/mm}$ ) of the square-wave grating was  $(6.1 \times \pi/4) \times 4/(3\pi)$ , or equivalently,  $6.1/3 \approx 2.0 \mu\text{m}$  (see (4)). The question then was whether a sinusoidal grating at  $5 \text{ c/mm}$  was detectable at an amplitude of  $2.0 \mu\text{m}$ . The answer could be found from the results of Exp. 1. In Fig. 9, the detection threshold for a sinusoidal grating at  $5 \text{ c/mm}$  was  $2.2 \mu\text{m}$ . It thus appeared that in Exp. 2, the sinusoidal and square-wave gratings at  $1.667 \text{ c/mm}$  became discriminable when the third harmonic component of the square-wave became strong enough to be detectable.

To visualize the comparison described above, we took the discrimination thresholds obtained from Exp. 2, shifted them up in frequency by a factor of 3, and scaled them down in amplitude by a factor 3, to obtain the amplitudes of the third harmonics of the square-wave gratings at the discrimination threshold (filled triangles in Fig. 12). These data points were then compared to the detection thresholds obtained from Exp. 1 (open circles in Fig. 12, replotted from Fig. 9). To the extent that the filled triangles were at or above the corresponding open circles in Fig. 12, we would conclude that the third harmonics were detectable. A visual inspection indicates that the data points at the higher spatial frequencies were quite similar. It appears quite plausible that as the amplitude of a square-wave grating increased, only the fundamental component was perceivable initially, and therefore, the

square-wave grating was indistinguishable from a sinusoidal grating. As the square-wave amplitude increased further, the amplitude of the third harmonic component reached its own detection threshold, thereby making it possible to discriminate the sinusoidal and square-wave gratings.

### 4.3 Discussion

In this experiment, we estimated the discrimination thresholds for sinusoidal versus square-wave gratings. The discrimination thresholds were compared to the detection thresholds obtained from Exp. 1, to test the hypothesis that the third harmonic components of the square-wave gratings became detectable at the discrimination thresholds. We found that our hypothesis was supported by the data obtained at the higher spatial frequencies. Consistent with the results obtained from Exp. 1, the data at the lower spatial frequencies did not conform to our hypothesis. The reasons are discussed in Section 6 when we consider the results from both Exps. 1 and 2 together.

The results obtained from Exps. 1 and 2 so far strongly suggest that the *detection* of square-wave gratings depends on the detection of its spectral components. An interesting question then is whether the *perception* of a grating consisting of multiple sinusoidal components (such as the square-wave grating used in the present study) depends on its spatial shape or the amplitudes of its spectral components only. Specifically, does the relative phase of the components making up the complex waveform matter? This led to the third experiment, where the participants compared gratings consisting of two superimposed sinusoidal components with different relative phases.

## 5 EXPERIMENT 3: DISCRIMINATION OF COMPLEX-WAVEFORM GRATINGS

The purpose of this experiment was to measure the discrimination performance with grating pairs consisting of superimposed sinusoidal components with different phases in order to ascertain whether complex-waveform gratings are discriminated based on waveform shapes or magnitudes of the spectral components.

### 5.1 Participants

Four participants (2 males and 2 females, age range 24-43 years old, average age 33 years old) took part in the experiment. One of the participants (P2) had participated in Exps. 1 and 2 earlier. All participants gave their written consent to the protocol approved by the Institutional Review Board at Purdue University.

### 5.2 Stimuli

Virtual texture gratings with two superimposed sinusoidal components were generated on the minitstick. The surface height map  $h(x)$  of the gratings was defined by (6) below

$$h(x) = A \sin\left(\frac{2\pi x}{\lambda}\right) + \frac{A}{3} \sin\left(\frac{6\pi x}{\lambda} + \phi\right), \quad (6)$$

where the additional parameter  $\phi$  denotes the relative phase between the two sinusoidal components. The feedback force was calculated according to (5) as in Exps. 1 and 2. Note the similarity between (4) and (6): the stimuli in Exp. 3 were

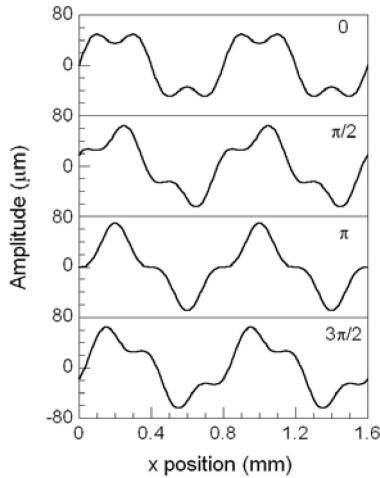


Fig. 13. Two-period samples of complex-waveform gratings used in Exp. 3 with  $A = 52.3 \mu\text{m}$  and  $\lambda = 0.8 \text{ mm}$  (see (6)). The values of  $\phi$  are shown in each panel.

designed to be consisted of the fundamental and the third harmonic components of a square-wave grating.

Two spatial periods, 0.8 and 12.8 mm, were chosen from the high and low spatial frequency regions, where our data were consistent and inconsistent with the hypotheses tested, respectively (see Figs. 10 and 12). The amplitudes were set to be 30 dB SL (sensation level); i.e., 30 dB above the detection threshold for the square-wave grating at the same spatial frequency. For example, the detection threshold for a square-wave grating at 1.25 c/mm was  $1.3 \mu\text{m}$  (Fig. 9). At 30 dB SL, the amplitude of the square-wave grating would be  $41.1 \mu\text{m}$ . The amplitude in (6) was, therefore, set to  $A = 41.1 \times 4/\pi = 52.3 \mu\text{m}$ . Fig. 13 shows four spatial waveforms calculated according to (6) with  $A = 52.3 \mu\text{m}$ ,  $\lambda = 0.8 \text{ mm}$ , and  $\phi = 0, \pi/2, \pi,$  and  $3\pi/2$ , respectively. The two waveforms with  $\phi = 0$  and  $\pi$  look the most different, hence, were chosen for direct comparison. The two waveforms with  $\phi = \pi/2$  and  $3\pi/2$  were also chosen for comparison because they were found to be most discriminable among a similar set of waveforms (see [21, Figs. 1 and 2]). Table 1 lists the parameter values for the four experimental conditions.

### 5.3 Procedure and Data Analysis

A one-interval two-alternative forced-choice signal detection paradigm with trial by trial correct-answer feedback was used [22]. On each trial, the participants received either

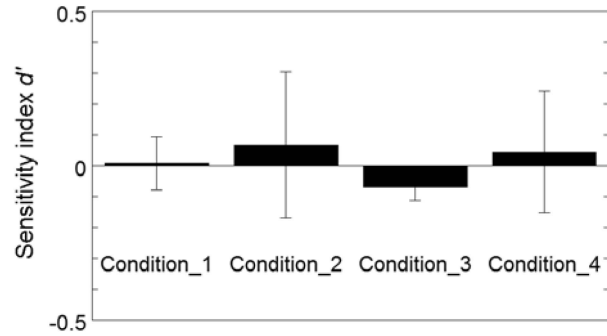


Fig. 14. Average  $d'$  values with standard deviations, for the four experimental conditions listed in Table 1.

the reference or the test stimulus. They were instructed to respond “1” to the reference stimulus and “2” to the test stimulus. Initial training was provided before each run. Each participant completed four 100-trial runs corresponding to the four experimental conditions. The order of the conditions was randomized for each participant. The participants wore sound attenuating earmuffs to eliminate any possible auditory cues.

Data from each condition formed a  $2 \times 2$  stimulus-response matrix consisting of 100 trials. Instead of calculating the percent-correct scores that are often confounded by participants’ response biases, we estimated the sensitivity index  $d'$  that provided a bias-free measure of the discriminability between the reference and the test gratings [22]. In this method of data processing, it is assumed that the underlying density functions associated with the two stimuli are normal and of equal variances (means  $M_1$  and  $M_2$ , and variance  $\sigma^2$ ). The sensitivity index  $d'$  is then defined as the normalized difference between the means:  $d' = (M_1 - M_2)/\sigma$ . For each experimental condition, the average and standard deviations of the  $d'$  values for the four participants were calculated. A  $d'$  value of 0.0, 1.0, or 2.0 corresponds to a percent-correct score of 50, 69, or 84 percent, respectively, assuming no response biases. For one-interval stimulus presentation,  $d' = 1$  is usually used as a performance criterion for defining discrimination threshold. Therefore, a  $d'$  value below 1.0 would be interpreted as the participants being unable to discriminate the reference and test stimuli [21].

### 5.4 Results and Discussion

Fig. 14 shows the  $d'$  values for the four conditions averaged across the four participants. It is clear that none of the

TABLE 1  
Experimental Conditions in Exp. 3

Condition	$\lambda$ (mm)	$A$ ( $\mu\text{m}$ )	Stimulus	$\phi$ (radian)
1	0.8	52.3	Reference	0
			Test	$\pi$
2	0.8	52.3	Reference	$\pi/2$
			Test	$3\pi/2$
3	12.8	213.4	Reference	0
			Test	$\pi$
4	12.8	213.4	Reference	$\pi/2$
			Test	$3\pi/2$

participants could discriminate the complex waveform pairs listed in Table 1.

These results indicate that surface gratings consisting of two sinusoidal components with different relative phases cannot be easily discriminated, thereby discounting the possibility that haptic gratings were discriminated based on the 3D height profiles. Note that the sinusoidal components making up the waveforms in Exp. 3 were all above human detection thresholds, therefore, the low  $d'$  values could not be attributed to the imperceptibility of the higher frequency (i.e., the third harmonic) components. The results obtained from Exp. 3 lend support to our assertion that the detection of a grating consisting of multiple sinusoidal components, such as a square-wave grating, is determined by the detection of its individual components. Furthermore, our data suggest that the relative phase between the sinusoidal components of a complex-waveform grating does not affect the perception of the gratings. Therefore, perception depends on the magnitudes of the spatial spectral components only, not the phases.

## 6 GENERAL DISCUSSION

The present study investigated the perception of virtual texture gratings containing multiple spectral components as represented by a Fourier series. We hypothesized that as the amplitude of a square-wave grating increased, the participants first perceived its fundamental component, then its third, fifth, etc., harmonic components. In Exp. 1, we measured the detection thresholds for virtual sinusoidal and square-wave texture gratings generated by a 3-DOF high position-precision force-feedback device. The results indicated that for spatial periods up to 6.4 mm, or equivalently, for spatial frequencies greater than 0.156 c/mm, the detectability of square-wave gratings could be predicted *quantitatively* from the detection thresholds of their corresponding fundamental components.

As far as we are aware, the detection thresholds measured in Exp. 1 are the first results ever reported for virtual sinusoidal and square-wave gratings. Louw et al. [23] reported haptic detection thresholds of Gaussian profiles using active touch of real samples. The thresholds were then converted to equivalent amplitudes of sinusoidal gratings with matched maximum slope (see details in the Appendix of [15]). The threshold amplitudes for sinusoidal gratings with spatial periods of 2.5, 5.0, and 10.0 mm were estimated to be approximately 0.64, 1.79, and 4.99  $\mu\text{m}$ , respectively ([15, pp. 1266-1267]). If we were to plot these three estimated thresholds on Fig. 9 at the corresponding spatial frequencies of 0.4, 0.2, and 0.1 c/mm, respectively, they would be much smaller than the detection thresholds measured at similar spatial frequencies in Exp. 1. The differences in our results and those of [23], [15] could be due to at least four significant differences in the two studies. First, Louw et al.'s study [23] used real samples that the participants could touch with the fingerpads of their index and middle fingers, whereas our present study simulated virtual gratings explored with a point-contact stylus. One can, therefore, argue that more information was available to the participants who touched real samples. Second, the thresholds obtained from Louw et al.'s study [23] corresponded to the 75 percent point on the psychometric function whereas ours corresponded to

the 79.4 percent point. This may potentially contribute to the higher thresholds in the present study due to the higher performance level required. Third, we explicitly modeled surfaces with multiple cycles of sinusoidal and square waveforms whereas Louw et al. [23] used samples with one cycle of Gaussian profile. It is possible that there was a masking effect with multiple cycles of waveforms. Finally, the amplitude thresholds estimated by Nefs et al. [15] were based on a conversion from the thresholds for Gaussian profiles to those for sinusoidal profiles by matching the maximum slope of the two profiles. Other conversion methods could conceivably lead to different threshold estimates.

In Exp. 2, we measured the discrimination threshold for pairs of virtual sinusoidal and square-wave gratings covarying in amplitude such that the amplitude of the square-wave's fundamental component always matched that of the sinusoidal grating. We found that at higher spatial frequencies, the square-wave gratings were initially indistinguishable from sinusoidal gratings at the same frequency until the square-wave's third harmonics were detectable. Furthermore, at lower spatial frequencies, the results from Exp. 1 also showed that the third (and possibly higher order) harmonic component of a square-wave grating was detectable before the fundamental component. Therefore, the square-wave grating was detectable as soon as the third harmonic was detectable, at an amplitude level that was lower than the detection threshold for the fundamental component. It also follows that the square-wave grating, once detectable, was never confused with a sinusoidal grating.

In both Exps. 1 and 2, the data at the lower spatial frequencies deviated from the expected values. This was actually to be expected, given the detection threshold versus spatial frequency curve measured in Exp. 1 (open circles in Fig. 9). Note that at low frequencies, the detection thresholds for sinusoidal gratings decreased rapidly as the spatial frequency increased, indicating better sensitivities at higher spatial frequencies. It was, thus, quite possible that given a square-wave grating at low spatial frequency, the participants were more sensitive to the third harmonic component than to the fundamental component even though the amplitude of the third harmonic was 1/3 of that of the fundamental. For example, the detection threshold for a sinusoidal grating at the lowest spatial frequency of 0.039 c/mm was 74.6  $\mu\text{m}$  (Fig. 9). The threshold at three times that frequency (0.119 c/mm) was about 14.0  $\mu\text{m}$  (interpolated linearly from the thresholds of 20.6  $\mu\text{m}$  at 0.078 and 7.8  $\mu\text{m}$  at 0.156 c/mm), which was less than 1/3 of 74.6  $\mu\text{m}$ . Therefore, we expect the third harmonic component of a square-wave grating at 0.039 c/mm to be detectable before the fundamental component reached its detection threshold.

Similar calculations can be performed on the fifth, seventh, etc., harmonic components. The point, however, is that at the lower spatial frequencies, a square-wave grating was never perceived as a sinusoidal grating at the same spatial frequency. The square-wave grating was detected initially by the detectability of its harmonics, *before* its fundamental component was detectable. This explains why, at lower spatial frequencies, the square-wave detection thresholds (filled squares in Fig. 9) were lower than the corresponding sinusoidal grating thresholds (open circles in Fig. 9), and the ratios in Fig. 10 were much bigger than  $4/\pi$ .

This also explains why, at lower spatial frequencies, the participants were able to discriminate sinusoidal and square-wave gratings at amplitude levels (filled triangles in Fig. 12) that were smaller than those predicted by our model, stipulating that the participants sensed the fundamental component of a square-wave grating first, then the harmonics (open circles in Fig. 12).

In Exp. 3, we further tested whether perception of a complex-waveform grating was determined by the *magnitudes* of its spatial spectral components alone, or was affected by the relative phase between the components as well. We restricted our stimuli to gratings consisting of two sinusoidal components similar to the fundamental and third harmonic components of a square-wave grating. Our results indicated that the participants could not distinguish gratings with the same component amplitudes but different relative phases.

Despite a large body of literature on the properties of mechanoreceptors in the skin, covering a range of topics from detection thresholds [8], [24] to functional mechanisms [25] to the perception of gratings [26], [27], [28], our present study is one of the first to explicitly investigate the superposition property of the somatosensory system using Fourier analysis (see also [8], [7]). The results of our study have implications for not only the mechanism of haptic perception but also engineering applications. If the human somatosensory system indeed performs a spectrum analysis of proximal stimuli, as our data seem to suggest, then the thresholds for complex signals could be predicted from the thresholds for the sinusoidal harmonic components. From an application point of view, it may not be necessary to transmit the higher frequency components of a haptic signal if their amplitudes are below human detection thresholds. It also appears that the relative phase of spectral components does not need to be preserved at threshold level. This perception-based approach can greatly ease the requirements on data transmission bandwidth without sacrificing the perceived quality of haptic signals at the receiver's end. A limitation of this approach is the range of spatial frequencies over which the method can be applied. Different waveforms (triangle, sawtooth, etc.) have different coefficients for the harmonic components, which dictate the relative detectability of the fundamental versus harmonic components. It is the goal of our future research to expand what we have learned in the present study by using additional types of waveforms for surface texture gratings and by rendering additional properties of virtual haptic surfaces.

## ACKNOWLEDGMENTS

The authors thank Dr. Roger Cholewiak for many useful discussions on the present study and commenting on earlier versions of the manuscript. They also thank Patrick Kalita for the data shown in Fig. 7. Dr. Daniel Leaird at Purdue University suggested and provided the stepper motor stage. The thoughtful comments from the reviewers are greatly appreciated. This research was partly supported by the US National Science Foundation (NSF) under grant nos. 0328984 and 0533908, and by a NASA award under grant no. NCC 2-1363. Partial results from Exp. 1 were presented at the World Haptics Conference 2007 [29].

## REFERENCES

- [1] S.A. Wall and W.S. Harwin, "Modelling of Surface Identifying Characteristics Using Fourier Series," *Proc. Conf. Am. Soc. Mechanical Engineers Dynamic Systems and Control Division*, vol. 67, pp. 65-71, 1999.
- [2] J.M. Weisenberger, M.J. Krier, and M.A. Rinker, "Judging the Orientation of Sinusoidal and Square-Wave Virtual Gratings Presented via 2-DOF and 3-DOF Haptic Interfaces," *Haptics-e: The Electronic J. Haptics Research*, vol. 1, <http://www.haptics-e.org>, 2000.
- [3] S. Choi and H.Z. Tan, "Perceived Instability of Virtual Haptic Texture. I. Experimental Studies," *Presence: Teleoperators and Virtual Environments*, vol. 13, pp. 395-415, 2004.
- [4] F.W. Campbell and J.G. Robson, "Application of Fourier Analysis to the Visibility of Gratings," *J. Physiology*, vol. 197, pp. 551-566, 1968.
- [5] J.C. Makous, R.M. Friedman, and C.J. Vierck, Jr., "A Critical Band Filter in Touch," *J. Neuroscience*, vol. 15, pp. 2808-2818, 1995.
- [6] H.T. Nefs, A.M.L. Kappers, and J.J. Koenderink, "Detection of Amplitude Modulation and Frequency Modulation in Tactile Gratings: A Critical Bandwidth for Active Touch," *Perception*, vol. 32, pp. 1259-1271, 2003.
- [7] S. Bensmaïa, M. Hollins, and J. Yau, "Vibrotactile Intensity and Frequency Information in the Pacinian System: A Psychophysical Model," *Perception & Psychophysics*, vol. 67, pp. 828-841, 2005.
- [8] S.J. Bolanowski, Jr., G.A. Gescheider, R.T. Verrillo, and C.M. Checkosky, "Four Channels Mediate the Mechanical Aspects of Touch," *J. Acoustical Soc. Am.*, vol. 84, pp. 1680-1694, 1988.
- [9] G.A. Gescheider, S.J. Bolanowski, and K.R. Hardick, "The Frequency Selectivity of Information-Processing Channels in the Tactile Sensory System," *Somatosensory and Motor Research*, vol. 18, pp. 191-201, 2001.
- [10] S. Bensmaïa and M. Hollins, "The Vibrations of Texture," *Somatosensory and Motor Research*, vol. 20, pp. 33-43, 2003.
- [11] S. Choi and H.Z. Tan, "Perceived Instability of Virtual Haptic Texture. II. Effect of Collision Detection Algorithm," *Presence: Teleoperators and Virtual Environments*, vol. 14, pp. 463-481, 2005.
- [12] S. Choi and H.Z. Tan, "Perceived Instability of Virtual Haptic Texture. III. Effect of Update Rate," *Presence: Teleoperators and Virtual Environments*, vol. 16, pp. 263-278, 2007.
- [13] H.Z. Tan, B.D. Adelstein, R. Traylor, M. Kocsis, and E.D. Hirtleman, "Discrimination of Real and Virtual High-Definition Textured Surfaces," *Proc. 14th Int'l Symp. Haptic Interfaces for Virtual Environment and Teleoperator Systems (HAPTICS '06)*, pp. 3-9, 2006.
- [14] M. Kocsis, H.Z. Tan, and B.D. Adelstein, "Discriminability of Real and Virtual Surfaces with Triangular Gratings," *Proc. Second Joint EuroHaptics Conf. and Symp. Haptic Interfaces for Virtual Environment and Teleoperator Systems (WHC '07)*, pp. 348-353, 2007.
- [15] H.T. Nefs, A.M.L. Kappers, and J.J. Koenderink, "Amplitude and Spatial-Period Discrimination in Sinusoidal Gratings by Dynamic Touch," *Perception*, vol. 30, pp. 1263-1274, 2001.
- [16] B.D. Adelstein, "Three Degree of Freedom Parallel Mechanical Linkage," US Patent 5,816,105, Oct. 1998.
- [17] R. Traylor, "Design of an Ethernet Enabled Embedded Controller for Stand-Alone Haptic Interfaces," master of science thesis, School of Electrical and Computer Eng., Purdue Univ., 2005.
- [18] H.Z. Tan, S. Yang, Z. Pizlo, P. Buttolo, and M. Johnston, "Manual Detection of Spatial and Temporal Torque Variation through a Rotary Switch," *IEEE Trans. Haptics*, vol. 1, no. 2, pp. 96-107, July-Dec. 2008.
- [19] H. Levitt, "Transformed Up-Down Methods in Psychoacoustics," *J. Acoustical Soc. Am.*, vol. 49, pp. 467-477, 1971.
- [20] M.R. Leek, "Adaptive Procedures in Psychophysical Research," *Perception & Psychophysics*, vol. 63, pp. 1279-1292, 2001.
- [21] S. Bensmaïa and M. Hollins, "Complex Tactile Waveform Discrimination," *J. Acoustical Soc. Am.*, vol. 108, pp. 1236-1245, 2000.
- [22] N.A. Macmillan and C.D. Creelman, *Detection Theory: A User's Guide*, second ed. Lawrence Erlbaum Assoc., 2004.
- [23] S. Louw, A.M.L. Kappers, and J.J. Koenderink, "Haptic Detection Thresholds of Gaussian Profiles over the Whole Range of Spatial Scales," *Experimental Brain Research*, vol. 132, pp. 369-374, 2000.
- [24] C.L. Van Doren, "The Effects of a Surround on Vibrotactile Thresholds: Evidence for Spatial and Temporal Independence in the Non-Pacinian I (NP I) Channel," *J. Acoustical Soc. Am.*, vol. 87, pp. 2655-2661, 1990.

- [25] K.O. Johnson, T. Yoshioka, and F. Vega-Bermudez, "Tactile Functions of Mechanoreceptive Afferents Innervating the Hand," *J. Clinical Neurophysiology*, vol. 17, pp. 539-558, 2000.
- [26] A.W. Goodwin and J.W. Morley, "Sinusoidal Movement of a Grating across the Monkey's Fingerpad: Representation of Grating and Movement Features in Afferent Fiber Responses," *The J. Neuroscience*, vol. 1987, pp. 2168-2180, 1987.
- [27] J.W. Morley, A.W. Goodwin, and I. Darian-Smith, "Tactile Discrimination of Gratings," *Experimental Brain Research*, vol. 49, pp. 291-299, 1983.
- [28] C.L. Van Doren, "A Model of Spatiotemporal Tactile Sensitivity Linking Psychophysics to Tissue Mechanics," *J. Acoustical Soc. America*, vol. 85, pp. 2065-2080, 1989.
- [29] S. Cholewiak and H.Z. Tan, "Frequency Analysis of the Detectability of Virtual Haptic Gratings," *Proc. 2007 World Haptics Conf. (WHC '07): The Second Joint EuroHaptics Conference and Symp. Haptic Interfaces for Virtual Environment and Teleoperator Systems*, pp. 27-32, 2007.



**Steven A. Cholewiak** received the bachelor's degree in psychology and physics from the University of Virginia (UVA) in 2006. During his undergraduate study at UVA, he was a research assistant at Gerald Clore's Social Psychology Laboratory, Timothy Salthouse's Cognitive Aging Laboratory, and Dennis Proffitt's Perception Laboratory. After graduation, he worked as a research associate at the Haptic Interface Research Laboratory with Hong Z. Tan at Purdue University. He is currently working toward the PhD degree in cognitive psychology and perceptual science at Rutgers University and is a National Science Foundation Integrative Graduate Education and Research Traineeship fellow. He has published two peer-reviewed conference papers and two posters under the study of Hong Z. Tan. His current research focuses on modeling haptic and visual perception.

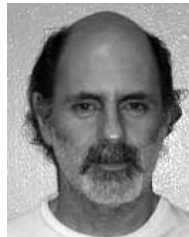


digital watermarking and haptics rendering.

**Kwangtaek Kim** received the bachelor's and master's degrees in electrical engineering from Korea University in 1998 and 2001, respectively. He is working toward the PhD degree in the School of Electrical and Computer Engineering at Purdue University since August 2005. After graduation, he worked as a research engineer in the field of digital image processing for several companies in Korea. His research interests include haptics-aware



**Hong Z. Tan** received the bachelor's degree in biomedical engineering from Shanghai Jiao Tong University in 1986, and the master's and doctorate degrees in electrical engineering and computer science from the Massachusetts Institute of Technology (MIT) in 1988 and 1996, respectively. She is currently an associate professor of electrical and computer engineering, with courtesy appointments in the School of Mechanical Engineering and the Department of Psychological Sciences. She was a research scientist at the MIT Media Lab from 1996 to 1998 before joining the Faculty at Purdue University. She is an associate editor of the journals *Presence*, *ACM Transactions on Applied Perception*, and the *IEEE Transactions on Haptics*. She was a co-organizer (with Blake Hannaford) of the International Symposium on Haptic Interfaces for Virtual Environment and Teleoperator Systems from 2003 to 2005. She served as the founding chair of the IEEE Technical Committee on Haptics, a home for the international interdisciplinary haptics research community, from 2006 to 2008. She was a recipient of the US National Science Foundation CAREER award from 2000 to 2004, and a coauthor of "Haptic feedback enhances force skill learning" that won the Best Paper Award at the 2007 World Haptics Conference. She has published more than 110 peer-reviewed articles in journals and conference proceedings and two book chapters. Her research focuses on haptic human-machine interfaces in the areas of haptic perception, rendering, and multimodal performance. She is a senior member of the IEEE and a member of the Psychonomic Society.



**Bernard D. Adelstein** received the PhD degree in mechanical engineering from MIT in 1989. He has been with the Human Systems Integration Division at the NASA Ames Research Center since 1991. His research has centered on the assessment of coupled human-system performance for multisensory virtual environments with a focus on understanding human perception of time delays and intermodal (haptic, visual, and auditory) asynchronies and on developing technologies to mitigate their impact on human performance. Recently, he has led NASA assessments of launch vibration impacts on astronaut performance. He cofounded (with Ed Colgate) the Annual Symposium on Haptic Interfaces for Virtual Environment and Teleoperator Systems in 1992 and has been on the editorial board of the journals *Presence* and *Haptics-e*. He is a member of the IEEE, the ASME, the Sigma Xi, and the AAAS.

► For more information on this or any other computing topic, please visit our Digital Library at [www.computer.org/publications/dlib](http://www.computer.org/publications/dlib).